

Graph-theoretical KMC Framework for Calculating Effective Diffusivity in TPBAR Components: Effective Diffusivity of Tritium in α -Zr Grain Boundaries

September 2022

G. Nandipati W. Setyawan D. J. Senior A. M. Casella

DISCLAIMER

This report was prepared as an account of work sponsored by an agency of the United States Government. Neither the United States Government nor any agency thereof, nor Battelle Memorial Institute, nor any of their employees, **makes any warranty, express or implied, or assumes any legal liability or responsibility for the accuracy, completeness, or usefulness of any information, apparatus, product, or process disclosed, or represents that its use would not infringe privately owned rights.** Reference herein to any specific commercial product, process, or service by trade name, trademark, manufacturer, or otherwise does not necessarily constitute or imply its endorsement, recommendation, or favoring by the United States Government or any agency thereof, or Battelle Memorial Institute. The views and opinions of authors expressed herein do not necessarily state or reflect those of the United States Government or any agency thereof.

PACIFIC NORTHWEST NATIONAL LABORATORY
operated by
BATTELLE
for the
UNITED STATES DEPARTMENT OF ENERGY
under Contract DE-AC05-76RL01830

Printed in the United States of America

Available to DOE and DOE contractors from
the Office of Scientific and Technical
Information,
P.O. Box 62, Oak Ridge, TN 37831-0062
www.osti.gov
ph: (865) 576-8401
fox: (865) 576-5728
email: reports@osti.gov

Available to the public from the National Technical Information Service
5301 Shawnee Rd., Alexandria, VA 22312
ph: (800) 553-NTIS (6847)
or (703) 605-6000
email: info@ntis.gov
Online ordering: <http://www.ntis.gov>

Graph-theoretical KMC Framework for Calculating Effective Diffusivity in TPBAR Components: Effective Diffusivity of Tritium in α -Zr Grain Boundaries

September 2022

G. Nandipati W. Setyawan D. J. Senor A. M. Casella

Prepared for
the U.S. Department of Energy
Under Contract DE-AC05-76RL01830

Pacific Northwest National Laboratory
Richland, Washington 99354

Abstract

We report the development of a computer simulation tool based on the *Graph-theoretical kinetic Monte Carlo (GT-KMC) approach* that can be used to simulate diffusion and derive effective diffusivity of species in complex structures of TPBAR components. The GT-KMC framework was implemented in AKSOME, an on-lattice self-learning kinetic Monte Carlo tool developed at PNNL and was previously used to study solute diffusion in metal alloys. This newly developed tool will be helpful in simulating atom diffusion and extracting their effective diffusivities in grain boundaries and interfaces in various TPBAR components. Once benchmarked, the tool will be used to simulate the diffusion of tritium (hydrogen) along grain boundaries in α -Zr using the activation energy barrier data previously obtained from Density Functional Theory calculations.

Acronyms and Abbreviations

1D	One-Dimensional
2D	Two-Dimensional
3D	Three-Dimensional
^3H	Tritium
AKSOME	Atomistic Kinetic Simulations of Microstructural Evolution
BCC	Body-Centered Cubic
CI-NEB	Climbing Image Nudged Elastic Band
DFT	Density Functional Theory
FCC	Face-Centered Cubic
GB	Grain Boundary
GT-KMC	Graph-Theoretical KMC
HCP	Hexagonal Close Packed
KMC	Kinetic Monte Carlo
MEP	Minimum Energy Path
NN	Nearest-neighbor
O	Octahedral
OI	Octahedral Interstitial
PNNL	Pacific Northwest National Laboratory
T	Tetrahedral
TI	Tetrahedral Interstitial
TPBAR	Tritium-Producing Burnable Absorber Rods
VASP	The Vienna Ab Initio Software Package

Acknowledgments

This work was funded by the National Nuclear Security Administration (NNSA) of the US Department of Energy (DOE) through the Tritium Technology Program at Pacific Northwest National Laboratory. This research was carried out using institutional computing resources at Pacific Northwest National Laboratory. PNNL is a multiprogram national laboratory operated by Battelle Memorial Institute for the US DOE under DE-AC06-76RLO 1830.

Contents

Abstract	iv
Acronyms and Abbreviations	v
Acknowledgments	vi
1.0 Introduction	1
2.0 Kinetic Monte Carlo	2
2.1 Algorithm	2
2.2 Lattice Mapping	3
3.0 Graph-Theoretical KMC Approach	4
3.1 Format of Databases	5
3.1.1 Simulation Cell	5
3.1.2 Activated Event Database	5
4.0 Results and Discussions	7
4.1 Benchmarking	7
4.2 Hydrogen Diffusion in α -Zr	8
4.3 Hydrogen Diffusion in $\Sigma7\{0001\}$ GB in α -Zr	10
5.0 Conclusions	11
6.0 References	12

Figures

1	Schematic diagram of the TPBAR showing the Ni-plated zircaloy-4 getter	1
2	(a) Illustration of a simple unsymmetrical lattice that can be visualized as an undirected connected graph, and the lines connecting them indicate a neighboring relationship. For example S_{19} is connected to sites $S_5, S_7, S_{10}, S_{13}, S_{24}$ while S_1 is connected to sites S_9, S_{13}, S_{20} . (b) Adjacency list of the lattice graph in the dot language format.	4
3	Shows top fifteen lines of the input file which input the simulation cell corresponding to the lattice shown in Fig. 2	6
4	Shows the first three lines of the activated event database corresponding to the lattice shown in Fig. 2	6
5	Schematic of the 2D square lattice and the corresponding activated event diffusion database used for benchmarking the code.	7
6	Mean square displacement vs. time for the 2D surface diffusion at 300 K based on the KMC simulation of 36937 steps	7

Tables

1	Activation energies for an H atom to hop between interstitial sites	8
2	Diffusivities of the hydrogen atom at 300, 400 and 500 K	9
3	H-atom migration energies and prefactors obtained via Arrhenius fitting	9
4	Diffusivities of hydrogen in Zr from previous experimental and modeling studies	9
5	Comparison of the diffusivities of hydrogen atoms in the bulk α -Zr and in the $\Sigma 7\{0001\}$ GB at 300, 400 and 500 K	10
6	Comparison of migration barrier and the prefactor for the H-atom migration in bulk and in the $\Sigma 7\{0001\}$ GB in α -Zr	10

1.0 Introduction

The TPBARs used in the US DOE's Tritium Readiness Program are designed to produce ^3H in commercial PWR fuel assemblies [1, 2]. As shown in Fig. 1, the TPBAR consists of a Zircaloy-4 getter tube to capture the tritium produced by the neutron irradiation of LiAlO_2 pellets [1, 2]. The getter is sandwiched with nickel plating to prevent the oxidation of its surfaces. At the reactor operating temperature ($\sim 300\text{ }^\circ\text{C}$), hydrogen diffuses mobile in the bulk $\alpha\text{-Zr}$. Grain boundaries (GBs) are widely accepted as fast diffusion pathways for solutes in metals. Generally, the same is expected, even in the case of hydrogen. However, the experimental data available on the enhancement of hydrogen diffusion along grain boundaries are contradictory [3–11]. Furthermore, to our knowledge, there are no experimental or modeling studies of hydrogen diffusion along grain boundaries in $\alpha\text{-Zr}$. In this report, we describe the development of the GT-KMC approach and the simulation of hydrogen in $\Sigma 7\{0001\}$ GB in $\alpha\text{-Zr}$.

On a regular lattice, it is possible to derive an analytical expression for effective diffusivity even when atom hops exhibit a wide range of activation energy barriers because hop-lengths and hop-directions do not change from one stable site to another. With regard to modeling, the two obvious methods to compute diffusivities along GBs are the molecular dynamics (MD) and accelerated molecular dynamics methods. However, the achievable simulation time is typically limited to less than $1.0\text{ }\mu\text{s}$. Another modeling method that is used to compute diffusivities is the kinetic Monte Carlo method (KMC). For a given system, when all the possible diffusion hops and their activation energies are known *a priori*, using the KMC method, it is possible to simulate diffusion for longer simulation times and compute diffusivities over a wider temperature range than by using the MD method. However, due to the complexity of crystal structures of GBs, a computationally expensive, the off-lattice KMC approach is generally used. In this report we describe and apply the *graph theoretical KMC (GT-KMC)* approach [18], facilitates the use of the *on-lattice* KMC approach to simulate diffusion in complex crystal geometries, particularly in GBs. We then use the *GT-KMC* approach to compute the H-atom diffusivity in the $\Sigma 7\{0001\}$ GB in $\alpha\text{-Zr}$ and compare them with their diffusivities in the bulk.

This report is organized as follows. In Section 2.0, we describe the KMC method and the use of the lattice mapping in the *on-lattice* KMC approach, GT-KMC approach is described in Section 3.0, results are discussed in Section 4.0 and the conclusions in Section 5.0.

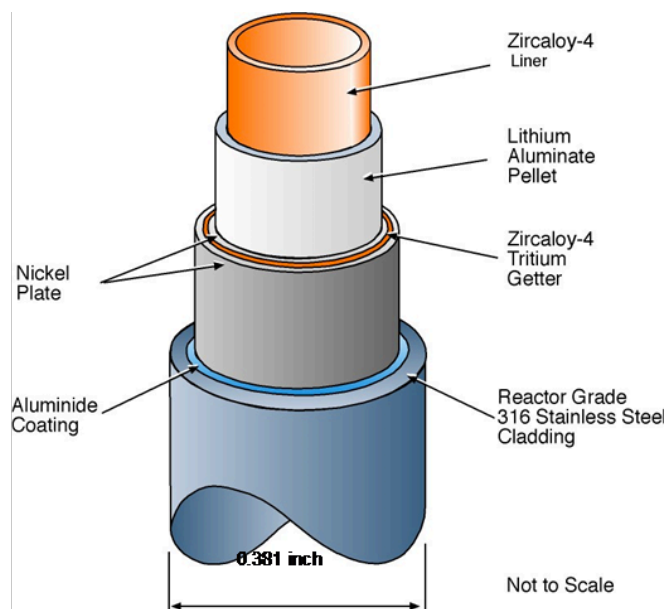


Figure 1: Schematic diagram of the TPBAR showing the Ni-plated zircaloy-4 getter

2.0 Kinetic Monte Carlo

Assuming that the interatomic potential gives an accurate description of the atomic forces for the material being modeled, the MD method can be used to accurately model the evolution of such systems on the atomic scale. The MD method simulates the time evolution of a system using classical equations of motion, and accurate integration of small time steps is required to resolve the atomic vibrations. Consequently, the total simulation time is typically limited to less than 1.0 μ s. However, in most material systems, dynamical or time evolution typically occurs through a series of *rare events* that occur at much longer time scales than atomic vibrations. Then the system's time evolution can be characterized by transitions from one state (potential energy minimum) to another, with long periods of inactivity between transitions. The KMC method uses this fact and evolves the system through state-to-state transitions instead of following the system trajectory throughout the vibrational time period. The KMC method, sometimes called *dynamic MC*, [15] is particularly efficient in simulating systems in which time evolution is characterized by *state-to-state* transitions [13, 14] and is a popular method for simulating a wide variety of dynamical processes [12–14].

In KMC simulations, transitions from one state to another are considered *Markovian*. That is, the transition rate ($\omega_{i \rightarrow j}$) depends only on the initial or present (i) and final states (j), and each transition is a stationary Poisson process, a good approximation for systems, which evolve via state-to-state transitions. In other words, the system spends enough time in its current state that it loses the memory of how it came to be in its current state. Starting from an initial configuration, the system is evolved using a stochastic algorithm that directly considers the energy barriers that govern the evolution of a system, which translates to a real-time scale. In material systems, the spatial arrangement of atoms corresponds to the *state* of the system, while the *atoms hop* from one stable location to another to the *transition* from one state to another. The transition rate between the states is usually determined using the transition state theory [16] as $\omega_{i \rightarrow j} = D_{ij}^0 \exp(-\mathcal{E}_{i \rightarrow j} / k_B T)$, where $\mathcal{E}_{i \rightarrow j}$, k_B , T , and D_{ij}^0 are the activation energy for the transition, the Boltzmann constant, the temperature, and the prefactor, respectively.

2.1 Algorithm

Starting from an initial configuration (i), the next state is chosen with a probability proportional to the transition rate ($\omega_{i \rightarrow j}$). The KMC algorithm based on the so-called *n-fold-way*, also known as Bortz-Kalos-Lebowitz (BKL), is outlined in the following steps:

- S1 Initialize the starting configuration (*i.e.* starting state of the simulation cell)
- S2 Set the simulation time $t_{\text{sim}} = 0$
 - For a restart of a previous simulation, $t_{\text{sim}} = t_{\text{start}}$
- S3 Identify and list all possible events (transitions) that can occur in the current state of the system and their rates calculated based on the TST.
- S4 Calculate the partial cumulative sums (in short called partial sums) of event rates: $S_i = \sum_{j=1}^i R_j$ for $i = 1, \dots, N$, where N is the total number of possible events in the current state.
 - The step can be thought of as calculating a cumulative probability distribution function from the discrete probability density function.

- Consequently, $S_N = R_T = \sum_{j=1}^N R_j$ is the total rate of events of the system in the current state.

S5 Generate a *uniform random number* $r_1 \in (0, 1]$, that is, between 0 and 1.

S6 Search for the value of j such that $S_{j-1} < r_1 R_T < S_j$.

S7 Perform *event* j .

- The system transitions to a new state or configuration.

S8 Generate another *uniform random number* $r_2 \in (0, 1]$.

S9 Advance the simulation time, $t_{\text{sim}}(\text{new}) = t_{\text{sim}}(\text{old}) + \Delta t$, where $\Delta t = -\ln(r_2) / R_T$.

- Δt is the time the system spent in the *old* state (or the *present state*) before transitioning to a *new* state. Hence, the algorithm is also called as the *residence-time algorithm*.

S10 Update rates of other events affected by the execution of *event* j .

S11 Go to *step* 3

Note that to execute step S3, all possible transitions out of the current state and their rates must be known *a priori*, and the method itself cannot predict them. Accordingly, all the possible transitions, along with their energetics, that can occur during the evolution of a system must be known *a priori*. Thus, the data on the possible transitions and their rates must be obtained either experimentally or derived from other simulation methods such as MD simulations or *ab initio* calculations.

2.2 Lattice Mapping

In materials systems, a *state* corresponds to a given arrangement of atoms, and a *state-to-state* transition entails a change in the location of the atoms. Accordingly, in diffusion-driven systems, a state-to-state transition is brought about by the diffusion of atoms hopping from one stable location to another. Most often, these stable sites are mapped onto a simple cubic lattice. KMC simulations using the approach of a fixed lattice (or a diced-grid) are termed *on-lattice* KMC simulations. Most often, but not always, this fixed lattice corresponds to the crystal structure of the material. Since the lattice points (or sites) are predefined, their numbers are always finite, and atoms are not allowed to be located in-between two lattice points. Alternatively, KMC simulations using the approach wherein atoms are allowed to occupy a continuous range of values are termed as *off-lattice* KMC simulations. Note that regardless of whether the coordinates of the atoms are of float-point or integer type, as long as the atoms in the simulations are restricted to specific points in space, these simulations are termed as the *on-lattice* KMC simulations. Implementing of the KMC method involves a lot of bookkeepings, and the on-lattice KMC approach is the method of choice when there is an *a priori* knowledge of the locations of the atoms, and the number of those sites is finite. The on-lattice KMC approach is computationally less expensive but comes at the expense of higher RAM usage.

3.0 Graph-Theoretical KMC Approach

The GT-KMC approach was originally proposed by Stamatakis *et. al* [17] to simulate chemical kinetics. Here we describe the application of the GT-KMC approach to simulate diffusion in material systems with complex geometry or systems with no symmetry. The GT-KMC approach makes it possible to use the on-lattice KMC approach to simulate diffusion in those systems when there are well-defined stable sites on which atoms can be located. With traditional mapping, stable sites in a material system with a regular crystal structure are mapped onto a cubic lattice, taking into account the symmetry in the system. A cubic lattice is a Bravais lattice, so the distances between neighboring lattice sites and the relative spatial geometry do not change from one lattice site to another. In contrast, with the GT-KMC

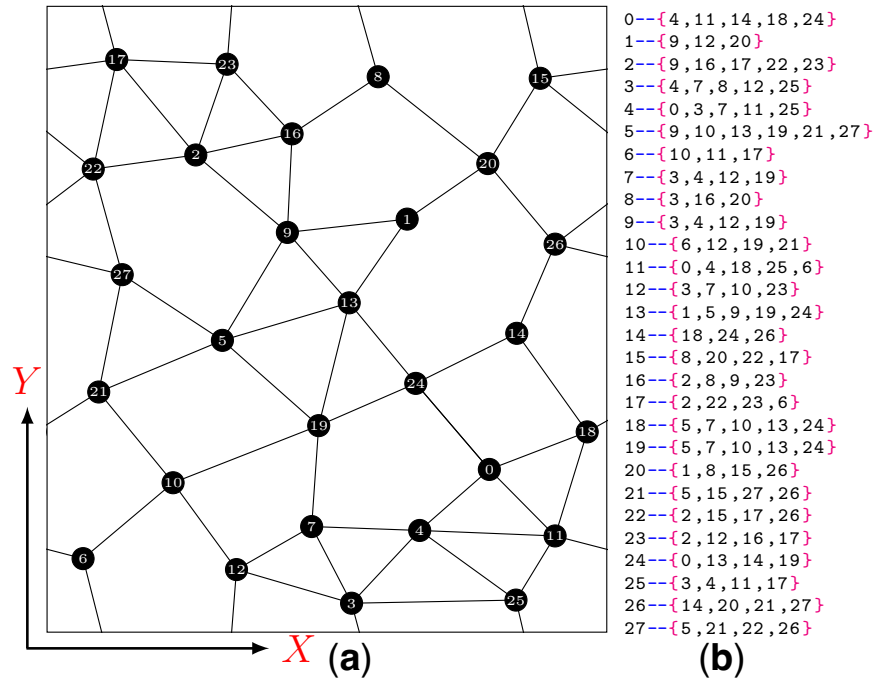


Figure 2: (a) Illustration of a simple unsymmetrical lattice that can be visualized as an undirected connected graph, and the lines connecting them indicate a neighboring relationship. For example \mathcal{S}_{19} is connected to sites $\mathcal{S}_5, \mathcal{S}_7, \mathcal{S}_{10}, \mathcal{S}_{13}, \mathcal{S}_{24}$ while \mathcal{S}_1 is connected to sites $\mathcal{S}_9, \mathcal{S}_{13}, \mathcal{S}_{20}$. (b) Adjacency list of the lattice graph in the dot language format.

approach, the number of neighboring sites and the distances between them, and their spatial geometry are allowed to be different from one lattice site to another. Each one of these sites (\mathcal{S}_i) is defined on the basis of its *position* and *type* i , and $i \in \{0, \dots, T\}$. i is also the site's index, and T is the total number of sites. Then the lattice is represented as a connected graph \mathcal{G} in which each vertex or node is a site index, and each edge introduces a neighboring relation between two sites.

$$\mathcal{G} = (\mathcal{S}, \mathcal{E}) \quad (1)$$

where $\mathcal{S} \in \{\mathcal{S}_0, \mathcal{S}_1, \dots, \mathcal{S}_T\}$ and \mathcal{E} contains two element subsets of \mathcal{S} , That is, $\mathcal{E}_{ik} = (\mathcal{S}_i, \mathcal{S}_k)$, where k is the indices of the neighboring sites of site i . Given the graph \mathcal{G} , one can form an adjacency list of the graph using \mathcal{E} , which encodes the lattice structure as a series of lists of all the connected sites of every lattice site.

Figure 2(a) shows a small unsymmetrical 2D lattice with 27 sites and the neighboring relation (denoted by the line connecting two sites), indicating that diffusion hop is allowed between the connected sites. Since no symmetry is assumed or expected, the number of connected sites (valency or degree) and how far they are located can be different for every site. Therefore, there

are as many different site types as there are sites in the lattice, and the index of a site can also represent its type. At any particular instance, a lattice site can be unoccupied or occupied and represents the state of the site (σ_i). That is, $\sigma_i = 1$ if the site is *occupied* and 0 if *unoccupied*. In a multi-atomic species system, one also needs to know the type of atomic species occupying a site. Therefore, its occupancy can be represented by the species number or the index of the atom occupying the site. For example, if j is the species number occupying a site i , then its state is given as $\sigma_i = j \in \{1, 2, \dots, \mathcal{N}_A\}$, where \mathcal{N}_A is the number of atomic species. Alternatively, one can also use the atom index to represent the occupancy or state of a site.

3.1 Format of Databases

The GT-KMC approach was implemented in AKSOME [19], a self-learning (SL) KMC code. In the present study, AKSOME will be used in non-SL mode; the data on possible diffusion hops and their activation energies are provided as input by the user. The present study focuses on hydrogen diffusion in a GB in α -Zr, and the hydrogen atom is the only diffusing entity. That is, the state of a site i is $\sigma_i = 1$ if it is occupied and 0 if empty. To use the GT-KMC approach, AKSOME requires two input files; the simulation cell containing the lattice sites and along with the information occupying those sites and a database of diffusion hops and their activation energies.

3.1.1 Simulation Cell

The simulations in the present study take the input from DFT calculations, and the format of the input configuration closely resembles VASP's POSCAR. In the present study, the input provides the list of all lattice sites and whether they are occupied or not. Figure 3 shows a snapshot of the input file and the description of its format used in the present study. The simulation cell in Fig. 3 contains only a single atom of `type = 1` located at `(0.0, 0.0, 0.0)`, while the remaining sites are empty and assigned `type = -1`. In the case of simulations with multiple atoms, then by specifying `line 5` as `1`, it is possible to specify both the `type` and `ID` of the atom occupying the site.

3.1.2 Activated Event Database

Figure 4 shows the first three lines of the activated event database, a required input to feed a simulation with information on atom hops and the corresponding activation energies. The database shown in Fig. 4 is for the simplest case when there is only one type of atom in the simulation cell, and the default is `type = 0`. Therefore, only the `site Id` is used to identify the appropriate energy barriers. Otherwise, both the `site Id` and `type` of the occupying atoms should be matched to assign the correct hops and their activation energies.

Note that the activated event database not only inputs the energetics of diffusion hops but implicitly also inputs the adjacency matrix. In this case, the adjacency implies that atoms are permitted to hop between the two sites or nodes.

```

Initial Configuration or input Cell
Format of the input file
1st Line: the overall scaling constant or lattice constant and the default value = 1.0
Lines 2,3,4 are the lattice vector of the simulation cell
ax ay az
bx by bz
cx cy cz
Line 5: No. of additional Items in each row (default = 0)
Line 6: No of nodes/sites in the simulation cell
x y z type (atom's type occupying the site)
-----
Any text above the hash symbol is considered as comments
#
1 0
2 9.63 0.0 0.0
3 0.0 9.63 0.0
4 0.0 0.0 9.63
5 0
6 28
7 0 0 0 0
8 3.21 0 0 -1
9 6.42 0 0 -1
10 0 3.21 0 -1
11 3.21 3.21 0 -1
12 6.42 3.21 0 -1
13 0 6.42 0 -1
14 3.21 6.42 0 -1
15 6.42 6.42 0 -1

```

Figure 3: Shows top fifteen lines of the input file which input the simulation cell corresponding to the lattice shown in Fig. 2

```

This is KMC DB for diffusion hops of an atom between lattice shown in the schematic
Format of the file
Line 1: Number of lattice sites
Line 2: <aty> <site Id> <D0> <Nhops> <Final Site Id1> <Ea1> <Final Site Id2> <Ea2>
where <aty> = atom type, <D0> = Prefactor <Nhops> = Number of hops, <Ea> = activation energy
-----
All lines above the hash symbol are considered as comments
#
1 28
2 0 0 1.0E+13 5 4 0.40 11 0.40 14 0.40 18 0.40 24 0.40
3 0 1 1.0E+13 3 9 0.40 12 0.40 20 0.40
4 0 2 1.0E+13 5 9 0.40 16 0.40 17 0.40 22 0.40 23 0.40

```

Figure 4: Shows the first three lines of the activated event database corresponding to the lattice shown in Fig. 2

4.0 Results and Discussions

4.1 Benchmarking

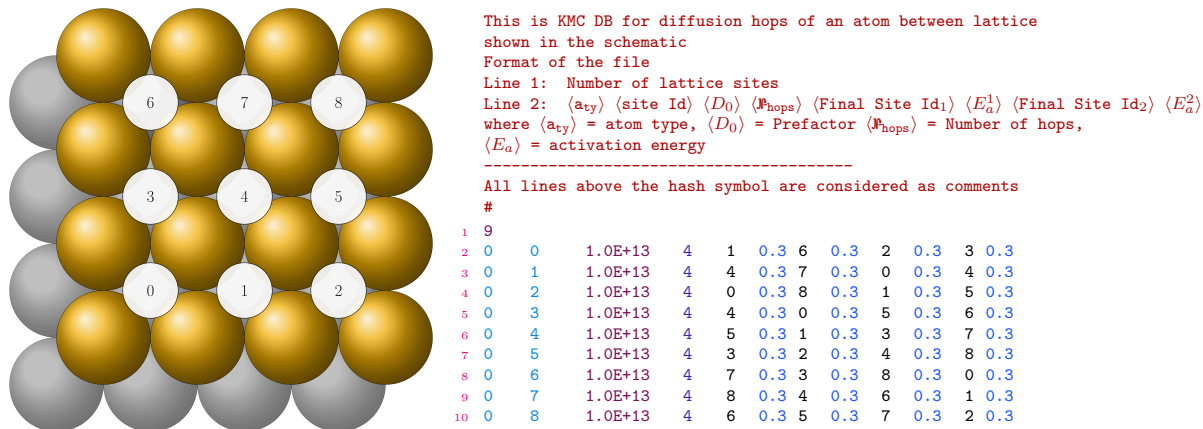


Figure 5: Schematic of the 2D square lattice and the corresponding activated event diffusion database used for benchmarking the code.

As noted earlier, the aim of the GT-KMC approach is to study diffusion in systems without symmetry. Hence, to benchmark the code, any material system can be used by ignoring any symmetry present in the system. That is, every individual hop between lattices must be explicitly specified. Therefore, to benchmark the newly developed code we simulated a simply 2D surface diffusion on a square lattice shown in Fig. 5 and assuming no symmetry is present. The activation energy between the sites is taken to 0.3 eV.

The diffusion coefficient (D) of a randomly diffusing entity, which in our case is a vacancy, is obtained using the Einstein equation: [20]

$$D = \lim_{t \rightarrow \infty} \frac{1}{2d\Delta t} \langle \Delta r(t)^2 \rangle$$

$$= \frac{1}{2d} \times \text{Slope of MSD Vs. Time} \quad (2)$$

where $\langle x^2 \rangle$ is the mean-square displacement and d is the diffusion dimensionality. Analytically, the diffusivity can be calculated using Eq. (3)

$$D = \frac{1}{2d} Z a_0^2 \Gamma \quad (3)$$

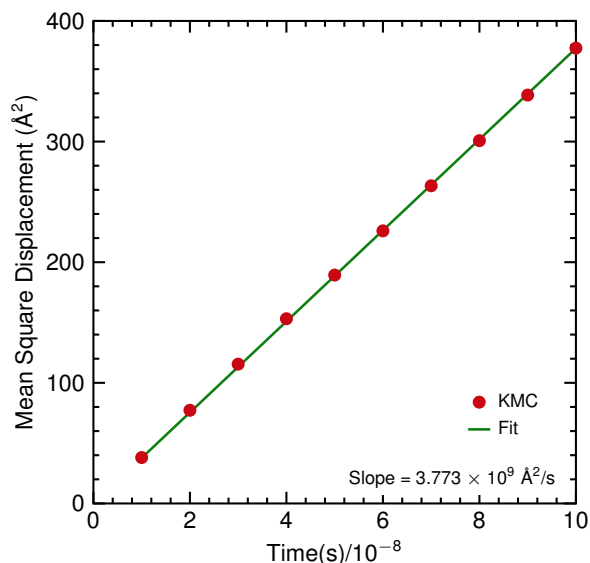


Figure 6: Mean square displacement vs. time for the 2D surface diffusion at 300 K based on the KMC simulation of 36937 steps

where d is the diffusion dimensionality, Z is the number of available pathways, a_0 is the lattice constant, and Γ is the hopping frequency along one of the available pathways. In the present case, the hopping frequency is taken to be the same along all available pathways.

In the case of 2D diffusion, $d = 2$. Using Eq. (2) the diffusivity of the atom diffusing on the 2D lattice shown in Fig. 5 at 300 K is $0.943 \times 10^9 \text{ \AA}^2 / \text{s}$ and using the Eq. (3), the diffusivity is $0.94 \times 10^9 \text{ \AA}^2 / \text{s}$. The negligible difference between the analytically calculated diffusivity and the one obtained from the KMC simulations shows that the newly developed code is working correctly.

4.2 Hydrogen Diffusion in α -Zr

Table 1: Activation energies for an H atom to hop between interstitial sites

Hop	E_a (eV)
$\text{T} \rightleftharpoons \text{T}$	0.09
$\text{O} \rightleftharpoons \text{O}$	0.51
$\text{O} \rightarrow \text{T}$	0.40
$\text{T} \rightarrow \text{O}$	0.42

Initially, we carried out simulations of hydrogen diffusion in bulk α -Zr to obtain hydrogen diffusivities in bulk α -Zr, which can be used for comparison with its diffusivities in $\Sigma 7\{0001\}$. In α -Zr, above room temperature, hydrogen atom diffuses via hopping between nearest-neighbor interstitial sites, with negligible contribution from quantum tunneling. In a hcp lattice, a hydrogen atom can occupy both the tetrahedral (T) and octahedral (O) interstitial sites. Accordingly, there are four possible hops, $\text{T} \rightleftharpoons \text{T}$, $\text{O} \rightleftharpoons \text{O}$, $\text{O} \rightarrow \text{T}$ and $\text{T} \rightarrow \text{O}$.

To simulate H-atom diffusion, we used a simulation box of $3 \times 3 \times 3$ unit cells containing 162 lattice sites corresponding to octahedral and tetrahedral interstitial sites. ($a_0 = 3.23 \text{ \AA}$ and $c/a_0 = 1.592$). Periodic boundary conditions were applied in all directions. A prefactor was taken to be $4 \times 10^{13} / \text{s}$, and the activation energies were taken from Ref. [21] and are shown in Table 1. Diffusivities obtained from the KMC simulations at 300, 400 and 500 K are shown in Table 2. It can be seen that hydrogen diffusion in α -Zr is anisotropic. However, the anisotropy is small. Furthermore, the hydrogen diffusivity is faster along the basal plane for temperatures less than 400 K but becomes faster along the c -axis for higher temperatures. Table 3 shows the effective migration barriers and prefactors obtained from the Arrhenius fit in the temperature range of 300-400 K. Table 4 shows the prefactors and migration barrier for hydrogen diffusion in bulk α -Zr from previous experimental and modeling studies. Tables 3 and 4 show that the prefactor from the KMC simulations has the same order of magnitude, while the migration barrier is within 0.1 eV as those obtained from experimental studies.

Table 2: Diffusivities of the hydrogen atom at 300, 400 and 500 K

Temperature (K)	Total Diffusivity D ($\text{\AA}^2/\text{s}$)	Basal Diffusivity D_{xy} ($\text{\AA}^2/\text{s}$)	c-axis Diffusivity D_z ($\text{\AA}^2/\text{s}$)	$\frac{D_{xy}}{D_z}$	No of KMC steps
300	7.63×10^6	7.70×10^6	7.49×10^6	1.03	6.5×10^6
400	3.58×10^8	3.61×10^8	3.53×10^8	1.02	1.0×10^7
500	3.39×10^9	3.31×10^9	3.54×10^9	0.94	3.0×10^7

Table 3: H-atom migration energies and prefactors obtained via Arrhenius fitting

Diffusivity	D_0 ($/10^{-3}$) (cm^2/s)	E_m (eV)
D	3.16	0.393
D_{xy}	3.06	0.392
D_z	3.65	0.398

Table 4: Diffusivities of hydrogen in Zr from previous experimental and modeling studies

References	Details	D_0 (cm^2/s)	Q (eV)
Kearns [22]	Longitudinal (expt.)	7.73×10^{-3}	0.470
	Transverse (expt.)	5.84×10^{-3}	0.446
	Radial (expt.)	7.90×10^{-3}	0.465
Someno [23]	α -Zr (expt., 450–700 °C)	4.15×10^{-3}	0.411
	β -Zr (expt., 870–1100 °C)	7.73×10^{-3}	0.370
Hashizume [24]	expt. (673—873 K K)	6.91×10^{-3}	0.461 ± 0.04
Mallett & Albrecht [25]	expt.	7.00×10^{-3}	0.306
Naito [25]	α -Zr (expt.)	6.70×10^{-3}	0.470
Mazzolai & Ryll-Nardzewski [26]	expt.	5.00×10^{-3}	0.500
Sawatsky [27]	α -Zircaloy-2 (expt.)	2.17×10^{-3}	0.363
Gulbransen & Andrew [28]	H in α -Zr (expt., 60–250 °C)	1.09×10^{-3}	0.494
	D in α -Zr (expt., 60–250 °C)	0.73×10^{-3}	0.494
Siripurapu <i>et al</i> [29]	MD (EAM)	1.69×10^{-2}	0.490
B. M. Lee & B. J. Lee	MD (MEAM 500—1550 K)	1.69×10^{-2}	0.502
Christensen <i>et al</i> [30]	MD	1.13×10^{-2}	-
Zhang <i>et al</i> [31]	DFT & KMC	5.55×10^{-3}	0.410

4.3 Hydrogen Diffusion in $\Sigma 7\{0001\}$ GB in α -Zr

In the case of hydrogen diffusion in a GB, we used a simulation cell containing 76 lattice sites or nodes, 28 sites are in the $\Sigma 7\{0001\}$ GB, 20 sites are in the near GB region, and the remaining are the tetrahedral and octahedral interstitial sites in the bulk. All activation energies for hops between different lattice sites were obtained from a previous study [21]. The GB is oriented along the xy -plane, hence the simulation box is periodic in the x - and y -directions. Since the probability of a hydrogen atom diffusing out of the GB is negligible, it diffuses only in 2D; in the xy -plane. Therefore, the dimensionality d in Eq. (3) is taken as 2. Table 5 shows the comparison of the diffusivities of hydrogen in the bulk α -Zr and in the $\Sigma 7\{0001\}$ GB at 300, 400 and 500 K. Table 6 shows the comparison of the migration barrier and the prefactor for the migration of H-atom in the bulk α -Zr and in the $\Sigma 7\{0001\}$ GB.

Table 5: Comparison of the diffusivities of hydrogen atoms in the bulk α -Zr and in the $\Sigma 7\{0001\}$ GB at 300, 400 and 500 K

Temperature K ($^{\circ}$ C)	Diffusivity (bulk) $\text{\AA}^2 / \text{s}$	Diffusivity ($\Sigma 7\{0001\}$ GB) $\text{\AA}^2 / \text{s}$
300 (23)	7.63×10^6	5.51×10^7
400 (127)	3.58×10^8	1.10×10^9
500 (227)	3.39×10^9	6.88×10^9

Table 6: Comparison of migration barrier and the prefactor for the H-atom migration in bulk and in the $\Sigma 7\{0001\}$ GB in α -Zr

	D_0 ($/10^{-3}$) (cm^2 / s)	E_m (eV)
Bulk	3.16	0.393
GB	0.95	0.312

From Table 5, it can be seen that the diffusivity of hydrogen within the GB is faster than in the bulk for all temperatures studied. At 300 K, diffusion along the GB is an order of magnitude faster than in the bulk. However, at 500 K, diffusion along the GB is only twice as fast as in the bulk. Therefore, at reactor temperatures ($\approx 300^{\circ}\text{C}$) the difference between bulk and GB diffusivities is expected to be even smaller. Accordingly, GB is unlikely to act as a short-circuit diffusion pathway for hydrogen.

5.0 Conclusions

We have developed a tool using the GT-KMC approach to simulate diffusion in grain boundaries or in other materials systems lacking symmetry. The approach was implemented in AKSOME, a self-learning (SL) KMC code developed at PNNL. In the present work, AKSOME was used in the non-SL mode; that is, all the possible processes and their rates are provided by the user. The newly developed code is benchmarked by simulating 2D diffusion on a square lattice, by ignoring system symmetries, and comparing KMC simulated diffusivities with those analytically calculated.

Next, we simulated hydrogen diffusion in bulk α -Zr, again ignoring system symmetries. We find that hydrogen diffusion is anisotropic. However, the anisotropy is small and changes with temperature. For temperatures below 500 K, the diffusion along the basal plane is faster. However, at higher temperatures diffusion along the c -axis is faster. Hence, at reactor temperatures, hydrogen is expected to diffuse faster along the c -axis.

Finally, we simulate the hydrogen diffusion along the $\Sigma\{0001\}$ GB. We find that the hydrogen diffusion is faster along the GB than in the bulk for all the temperatures studied. However, with increasing temperature, the difference in diffusivities decreases. At 500 K both diffusivities have the same order of magnitude and GB diffusivity is only twice as fast as the bulk diffusivity. Therefore, at reactor temperature, it is unlikely that hydrogen diffusion would be significantly faster along the $\Sigma\{0001\}$ GB than in the bulk and, in turn, as a short-circuit diffusion pathway. However, it is important to note that the hydrogen diffusivity along the GB would strongly depend on character of the GB, such as the GB energy and the excess volume [33, 34].

6.0 References

- [1] K. A. Burns, E. F. Love, C. K. Thornhill, *Description of the Tritium-Producing Burnable Absorber Rod For the Commercial Light Water Reactor*, TTQP-1-015 Rev 19, PNNL-22086, February, 2012
- [2] D. J. Senor, *Recommendations for Tritium Science and Technology Research and Development in Support of the Tritium Readiness Campaign*, TTP-7-084, PNNL-22873, October, 2013
- [3] R. D. Calder, T.S. Elleman, K. Verghese, *Grain Boundary Diffusion of Tritium in 304- and 316-Stainless Steels*, J. Nucl. Mater. **46** (1973) 46
- [4] A. M. Brass, A. Chanfreau, *Accelerated Diffusion of Hydrogen along Grain Boundaries in Nickel*, Acta Mat. **44** (1996) 3823
- [5] B. Ladna, H. K. Birnbaum, *SIMS Study of Hydrogen at the Surface and Grain Boundaries of Nickel Bicrystals*, Acta Metall. **35** (1987) 2537
- [6] A. Oudriss, J. Creus, J. Bouhattate, E. Conforto, C. Berziou, C. Savall, X. Feaugas, *Grain Size and Grain-Boundary Effects on Diffusion and Trapping of Hydrogen in Pure Nickel*, Acta Mat. **60** (2012) 6814-6828
- [7] A. Oudriss, J. Creus, J. Bouhattate, C. Savall, B. Peraudeau, X. Feaugas, *The Diffusion and Trapping of Hydrogen along the Grain Boundaries in Polycrystalline Nickel*, Scr Mater. **66** (2012) 37
- [8] M. Koyama, D. Yamasaki, T. Magashima, C. C. Tasan, K. Tsuzaki, *In-situ Observations of Silver-Decoration Evolution under Hydrogen Permeation: Effects of Grain Boundary Misorientation on Hydrogen Flux in Pure Iron*, Scripta Mat. **129** (2017) 48
- [9] B. Chew, F. T. Fabling, *The Effect of Grain Boundaries on the Low-Temperature Diffusion of Hydrogen in Decarburized Mild Steel*, Met. Sci. J. **6** (1972) 140
- [10] T. Tsuru, R. M. Latanision, Scripta Metall. **16** (1982) 575
- [11] M. D. Danford, *The Role of Grain Boundaries in Hydrogen Diffusion in Metals at 25 °C*, NASA Technical Memorandum 108407 (1993).
- [12] J.G. Amar, *The Monte Carlo Method in Science and Engineering*, Comput. Sci. Eng **8** (2006), 9
- [13] A. F. Voter, *Introduction to the kinetic Monte Carlo method* Rad. Effects Solids (NATO Sci Ser). **235** (2007) 1
- [14] M. Andersen, C. Panosetti, K. Reuter, *A Practical Guide to Surface Kinetic Monte Carlo Simulations* Front. Chem. **7** (2019), 202
- [15] K. A. Fichthorn, W. H. Weinberg, *Theoretical Foundations of Dynamical Monte Carlo Simulations*, J. Chem. Phys., **95** (1991) 1090
- [16] G. H. Vineyard, *Frequency Factors and Isotope Effects in Solid State Rate Processes*, J. Phys. Chem. Solids, **3**,(1957) 121
- [17] A. B. Bortz, M. H. Kalos, J. L. Lebowitz, *A New Algorithm for Monte Carlo Simulation of Ising spin systems*, J. Comput. Phys., **17** (1975) 10
- [18] M. Stamatakis and D. G. Vlachos, *A graph-theoretical kinetic Monte Carlo framework for on-lattice chemical kinetics*, J. Chem. Phys. **134** (2011) 214115
- [19] G. Nandipati, N. Govind, A. Andersen, A. Rohatgi, *"Self-learning kinetic Monte Carlo Simulations of AI diffusion in Mg,"* J. Phys: Condens. Matter **28** (2016) 155001
- [20] A. Einstein, Ann. d. Phys **17** (1905) 549
- [21] W. Setyawan, C. H. Henager, *"Modeling Thermodynamic Content of Tritium in Grain Boundaries of*

Zircaloy-4 Getter” PNNL-xxxx, Sep 2019 (in preparation)

- [22] J. J. Kearns, *Diffusion coefficient of hydrogen in alpha zirconium, Zircaloy-2 and Zircaloy-4*, J. Nucl. Mater. **43** (1972)330–8
- [23] M. Someno, *Hydrogen absorption of zirconium and measurement of diffusion coefficient* Nippon Kin-zoku Gakkaishi, **24** (1960) 249–53
- [24] K. Hashizume, *et. al, Application of Discharge Implantation Method to Measurement of Diffusion Co-efficient of Hydrogen Isotopes in Zirconium*,J. Nucl. Sci. Technol., **31** (1994) 1295
- [25] M. W. Mallett and W. M. Albrecht, *Low-Pressure Solubility and Diffusion of Hydrogen in Zirconium* J. Electrochem. Soc. **104** (1957) 142–6
- [26] S. Naito, *Kinetics of hydrogen absorption by α -zirconium* J. Chem. Phys. **79** (1983) 3113–20
- [26] F. Mazzolai, J. Ryll-Nardzewski, *An anelastic study of the diffusion coefficient of hydrogen in α -zirconium* J. Less-Common Met. **49** (1976) 323–7
- [27] A. Sawatzky, *The diffusion and solubility of hydrogen in the alpha phase of zircaloy-2* J. Nucl. Mater. **2** (1960)62–8
- [28] E. A. Gulbransen, K. F. Andrew, *Diffusion of Hydrogen and Deuterium in High Purity Zirconium*, J. Electrochem. Soc. **101** (1954) 560–6
- [29] R. K. Siripurapu, B. Szpunar, J. A. Szpunar, *Molecular Dynamics Study of Hydrogen in α -Zirconium*, Int. J. Nucl. Energy **2014** (2014) 912369
- [30] B. M. Lee, B. J. Lee, *A Comparative Study on Hydrogen Diffusion in Amorphous and Crystalline Metals Using a Molecular Dynamics Simulation*, Metall Mater Trans A **45** (2014) 2906–2915
- [31] M. Christensen, *et. al* 2015 *Zirconium in the Nuclear Industry* vol.17 (Hyderabad: ASTM International) pp 55–92
- [32] Y. Zhang, C. Jiang and X. Bai, *Anisotropic hydrogen diffusion in α -Zr and Zircaloy predicted by accelerated kinetic Monte Carlo simulations*, Sci. Rep. **7** (2017) 41033
- [33] X. Liu, W. Xie, W. Chen, H. Zhang, *Effects of Grain Boundary and Boundary Inclination on Hydrogen Diffusion in α -iron*, J. Mater. Res., **26** (2011) 2735
- [34] D. Di Stefano, M. Mrovec, C. Elsässer, *First-Principles Investigation of Hydrogen Trapping and Diffusion at Grain Boundaries in Nickel* Acta Mater, **98** (2015) 306-312

Pacific Northwest National Laboratory

902 Battelle Boulevard
P.O. Box 999
Richland, WA 99352
1-888-375-PNNL (7675)

www.pnnl.gov